REFERENCES

1. W.C. Chew and Y.M. Wang, Reconstruction of two-dimensional permittivity distribution using the distorted Born iterative method, IEEE Trans Med Imaging MI 9 (1990), 218–225.
2. T. Harada, D.J.N. Wall, T. Takenaka, and T. Tanaka, Conjugate gradient method applied to inverse scattering problem, IEEE Trans Antennas Propag 43 (1995), 784–792.
3. A. Franchois and C. Pichot, Microwave imaging in complex permittivity reconstruction with a Levenberg-Marquart method, IEEE Trans Antennas Propag 45 (1997), 203–214.
4. M. Norgren and S. He, A gradient-based optimization approach to the inverse problem for multilayered structures, Int J Appl Electromagn Mech 10 (1999), 315–335.
5. S. Caorsi, A. Massa, and M. Pastorino, Numerical assessment concerning a focused microwave diagnostic method for medical applications, IEEE Trans Microwave Theory Tech 48 (2000), 1815–1830.
6. A. Abubakar, P.M. Van den Berg, and J.J. Mallorqui, Imaging of biomedical data using a multiplicative regularized contrast source inversion method, IEEE Trans Microwave Theory Tech 50 (2002), 1761–1771.
7. T. Isernia, L. Crocco, and M. D'Urso, New tools and series for scattering problems in lossy media, IEEE Trans Geosci Remote Sensing Lett 1 (2004), 327–331.
8. P. Rocca, M. Benedetti, M. Donelli, D. Franceschini, and A. Massa, Evolutionary optimization as applied to inverse scattering problems, Inverse Prob 25 (2009), 1–41.
9. G. Oliveri, A. Randazzo, M. Pastorino, and A. Massa, Electromagnetic imaging within the contrast-source formulation by means of the multiscaling inexact Newton method, J Opt Soc Am A 29 (2012), 945–958.
10. M. Moghaddam and W.C. Chew, Study of some practical issues in inversion with the Born iterative method using time-domain data, IEEE Trans Antennas Propag 41 (1993), 177–184.
11. S. He, P. Fuks, and G.W. Larson, An optimization approach to time-domain electromagnetic inverse problem for a stratified dispersive and dissipative slab, IEEE Trans Antennas Propag 44 (1996), 1277–1282.
12. T. Takenaka, H. Zhou, and T. Tanaka, Inverse scattering for a three-dimensional object in the time domain, J Opt Soc Am A 20 (2003), 1867–1874.
13. S. He, S. Ström, and V.H. Weston, Time domain wave-splittings and inverse problems, Oxford University Press, Oxford, 1998.
14. M. Gustafsson and S. He, An optimization approach to two-dimensional time domain electromagnetic inverse problems, Radio Sci 35 (2000), 525–536.
15. T. Takenaka and T. Moriyama, Inverse scattering approach based on the field equivalence principle: inversion without a priori information on incident fields, Opt Lett 37 (2012), 3432–3434.
16. C.A. Balanis, Advanced engineering electromagnetics, Ch. 7, Wiley, New York, 1989.
17. P. Kosmas and C.M. Rappaport, Time reversal with the FDTD method for microwave breast cancer detection, IEEE Trans Microwave Theory Tech 53 (2005), 2317–2323.

VERY-LOW-PROFILE DUAL-WIDEBAND LOOP ANTENNA FOR LTE TABLET COMPUTER

Kin-Lu Wong and Meng-Ting Chen
Department of Electrical Engineering, National Sun Yat-sen University, Kaohsiung 80424, Taiwan; Corresponding author: wongkl@ema.ee.nsysu.edu.tw

Received 30 May 2014

ABSTRACT: *A very-low-profile (8 mm in height), small-size (8 × 3 × 40 mm^3), and dual-wideband loop antenna suitable for applications in the LTE tablet device such as a tablet computer is presented. Dual-wideband operation of the proposed loop antenna is achieved using a wideband feed structure formed by a coupling feed, a high-pass matching circuit, and a tuning inductor. The coupling feed leads to successful excitation of a quarter-wavelength loop mode in the desired lower band. The high-pass matching circuit causes an additional resonance occurred near the excited quarter-wavelength loop mode to widen the low-band bandwidth to cover the 698–960 MHz band. The tuning inductor can adjust the frequency ratio of the first two higher-order loop modes to form a wide higher band to cover the 1710–2690 MHz band. Dual-wideband operation of the proposed loop antenna for the LTE operation is hence obtained. Details of the proposed loop antenna are addressed. Working principle of the antenna, especially the function of the wideband feed structure thereof, is described. Experimental results of the fabricated prototype are also presented.* © 2015 Wiley Periodicals, Inc. Microwave Opt Technol Lett 57:141–146, 2015; View this article online at wileyonlinelibrary.com. DOI 10.1002/mop.28802

Key words: *mobile antennas; tablet computer antennas; LTE antennas; very-low-profile antennas; loop antennas; dual-wideband antennas; small-size antennas*

1. INTRODUCTION

For the tablet device such as the tablet computer to achieve the LTE operation, the embedded antenna with a very low profile (8 mm or less in height) [1] is becoming very attractive and demanded for practical applications. This is mainly because the spacing or clearance region between the display panel and the device frame in modern tablet computers is becoming narrower to achieve a more appealing device appearance for the user. It is also noted that although some interesting low-profile LTE tablet computer antennas have been recently reported to cover the 698–960 and 1710–2690 MHz bands [1–15], many of them requires a height of at least 10 or 15 mm above the top edge of the device ground plane [2–15]. This is mainly because the coupling between the antenna and the device ground plane will quickly increase, when the antenna height decreases, especially for the antenna height less than 10 mm. The increased coupling will lead to large variations in the antenna's input impedance, hence making it difficult in achieving acceptable impedance matching over a wide bandwidth.

Recently, for achieving a very low profile of 8 mm for the LTE tablet computer antenna, the design using a two-strip antenna formed by a driven strip and a shorted parasitic strip has been applied [1]. In such a design, the antenna occupies a volume of 8 × 3.8 × 50 mm^3. To achieve acceptable impedance matching over two wide operating bands of 698–960 and 1710–2690 MHz, the two-strip antenna requires a long lateral length of 50 mm along the top edge of the device ground plane of the tablet computer.

In this article, we present a promising dual-wideband loop antenna with a wideband feed structure formed by a coupling feed, a high-pass matching circuit, and a tuning inductor to achieve a very low profile of 8 mm and a small size of 8 × 3 × 40 mm^3. The antenna's occupied size is smaller than that in [1], and the antenna can cover the 698–960 and 1710–2690 MHz bands for the LTE operation. Details of the antenna structure are addressed, and working principle of the antenna, including the working principle of the wideband feed structure, are described in this study. The antenna was also fabricated and tested. The experimental results are presented and discussed.

2. PROPOSED ANTENNA

Figure 1 shows the geometry of the proposed very-low-profile dual-wideband loop antenna for the LTE tablet computer. Photos

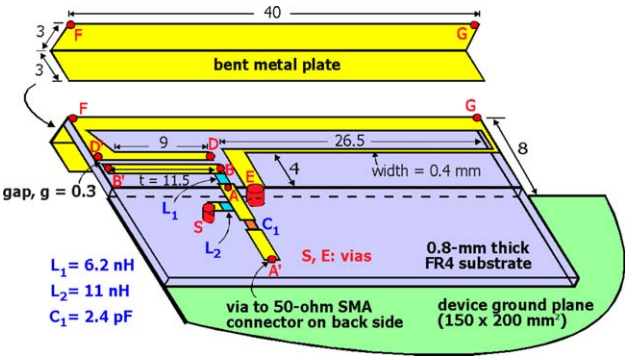

Figure 1 Geometry of the very-low-profile dual-wideband loop antenna for the LTE tablet computer. [Color figure can be viewed in the online issue, which is available at wileyonlinelibrary.com]

of the fabricated antenna in the experimental study are also shown in Figure 2 to provide a more clear view of the proposed antenna. The antenna is mounted along the top edge (long edge) and flushed to one corner of the device ground plane of a 9.7-inch tablet computer. The device ground plane size is 150 × 200 mm^2. The antenna is formed by a printed metal pattern and a bent metal plate. The printed metal pattern is disposed on a 0.8-mm thick FR4 substrate of relative permittivity 4.4 and loss tangent 0.024. The bent meal plate is cut from a 0.2-mm thick copper plate. The antenna occupies a volume of 8 × 3 × 40 mm^3 above the top edge of the device ground plane. Note that with the bent metal plate to increase the antenna's low-band bandwidth, the antenna is still with a thin thickness of 3 mm, which is acceptable for applications in modern slim tablet computers.

The antenna is mainly a loop antenna formed by a loop strip (section D′FGE) fed by a wideband feed structure. The loop

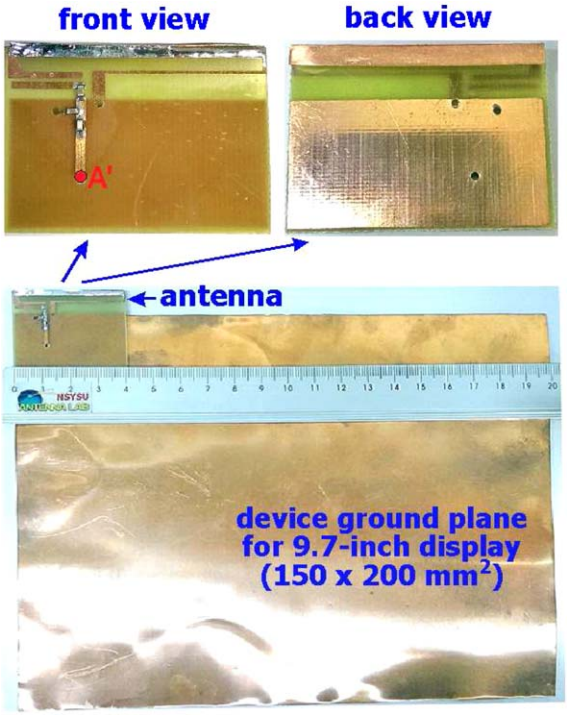

Figure 2 Photos of the fabricated antenna. [Color figure can be viewed in the online issue, which is available at wileyonlinelibrary.com]

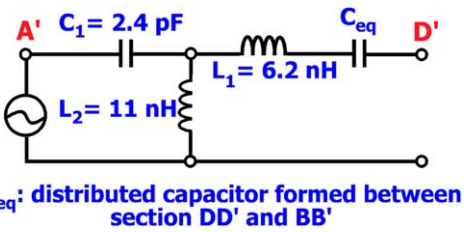

Figure 3 Equivalent circuit model of the feed structure. [Color figure can be viewed in the online issue, which is available at wileyonlinelibrary.com]

strip has a length of about 80 mm, close to 0.25 wavelength at 900 MHz. The wideband feed structure includes a coupling feed, a high-pass matching circuit (chip capacitor $C_1 = 2.4$ pF, chip inductor $L_2 = 11$ nH), and a tuning inductor (chip inductor $L_1 = 6.2$ nH). The equivalent circuit model of the feed structure is shown in Figure 3. The coupling feed is formed between sections DD′ and BB′, which has a gap width g of 0.3 mm and can be represented as a distributed capacitor C_{eq} in the equivalent circuit model. With the coupling feed, the quarter-wavelength loop mode can be successfully excited [16–18] in the desired lower band. Compared to the traditional loop antenna that is mainly operated at the half-wavelength loop mode as the fundamental or lowest resonant mode [19], the loop antenna in this study can have a decreased size for the LTE operation in the 698–960 MHz band.

Note that with the bent metal plate connected to the loop strip, although the achievable bandwidth of the quarter-wavelength loop mode can be increased, it is still far from covering the desired lower band. By aided with the high-pass matching circuit, an additional resonance near the excited quarter-wavelength loop mode can be generated to effectively widen the antenna's low-band bandwidth to cover the 698–960 MHz band. It should be noted that in practical applications, the three circuit elements L_1, L_2, and C_1 can be disposed on the system circuit board of the tablet computer. The occupied area for the circuit elements is usually very small and can generally be negligible [11].

Higher-order loop modes can also be generated for the proposed antenna. The tuning inductor L_1 can adjust the frequency ratio of the first two higher-order loop modes, such that a wide higher band can be obtained to cover the 1710–2690 MHz band. Hence, the proposed antenna can provide a dual-wideband operation to cover the LTE lower and higher bands of 698–960 and 1710–2690 MHz. Detailed working principle is addressed in Section 3.

3. WORKING PRINCIPLE

To analyze the antenna's working principle, Figure 4 shows the simulated return loss for the proposed antenna, the case without the tuning inductor L_1 and the high-pass matching circuit formed by L_2 and C_1 (denoted as Ant1), and the case without the high-pass matching circuit formed by L_2 and C_1 (denoted as Ant2). The full-wave electromagnetic field simulator HFSS version 15 is used to obtain the simulated results [20]. For Ant1, in which the three circuit elements (L_1, L_2, C_1) are not present, a resonant mode occurred at about 800 MHz is seen. This resonant mode is the quarter-wavelength loop mode excited with the aid of the coupling feed [16–18], which is represented as an equivalent distributed capacitor C_{eq} shown in Figure 3. In the desired higher band, a resonant mode is also occurred at about 2100 MHz, which is the antenna's first higher-order resonant

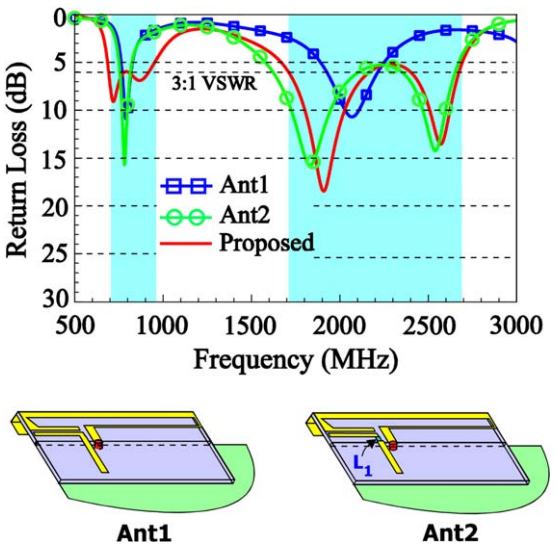

Figure 4 Simulated return loss for the proposed antenna, the case without the tuning inductor L_1 and the high-pass matching circuit formed by L_2 and C_1 (Ant1), and the case without the high-pass matching circuit formed by L_2 and C_1 (Ant2). [Color figure can be viewed in the online issue, which is available at wileyonlinelibrary.com]

mode. Note that the obtained bandwidths in the lower and higher bands are far from covering the desired LTE operation (see the two shaded frequency regions in the figure).

Simply by adding a tuning inductor L_1 of 6.2 nH to Ant1 (i.e., Ant2 is formed), a second higher-order resonant mode is shifted from higher frequencies to be at about 2600 MHz, while the first higher-order resonant mode is moved to be at about 1900 MHz. In this case, a wide higher band covering the LTE high band of 1710–2690 MHz is obtained. Then, by further adding a high-pass matching circuit to Ant2 (i.e., the proposed antenna), an additional resonance occurred in the desired lower band is obtained, which combines with the quarter-wavelength loop mode to form a wide lower band covering the LTE low band of 698–960 MHz. Also, the added high-pass matching circuit shows small effects on the high-band performance of the antenna. This makes it easy and convenient for the antenna to achieve LTE dual-wideband operation. Also note that for the proposed antenna, although there are some frequencies with return loss slightly less than 6 dB (3:1 VSWR), the obtained measured antenna efficiency is better than 40% in the lower band and better than 56% in the higher band, which is acceptable for practical applications [11]. The simulated and measured antenna efficiencies will be discussed in Section 5.

To show the effects of the tuning inductor (L_1) and the high-pass matching circuit (L_2, C_1) on the input impedance variations more clearly, Figure 5 shows the simulated input impedance on the Smith chart for Ant1 (curve 1), Ant2 (curve 2), and the proposed antenna (curve 3). Results for the frequency ranges of 690–1000 MHz and 1600–2700 MHz are presented in Figures 5(a) and 5(b), respectively. In the lower band, results of Ant1 and Ant2 show small variations (curve 1 vs. curve 2). This indicates that the tuning inductor has small effects on the antenna's low-band performance. Once the high-pass matching circuit is added, the dual-resonance behavior for the input impedance is seen (see curve 3) in the desired lower band, which has a wide operating band for the LTE low-band operation. This bandwidth-enhancement effect is related to the generation of a parallel resonance near an existing resonant mode [21–24]. In

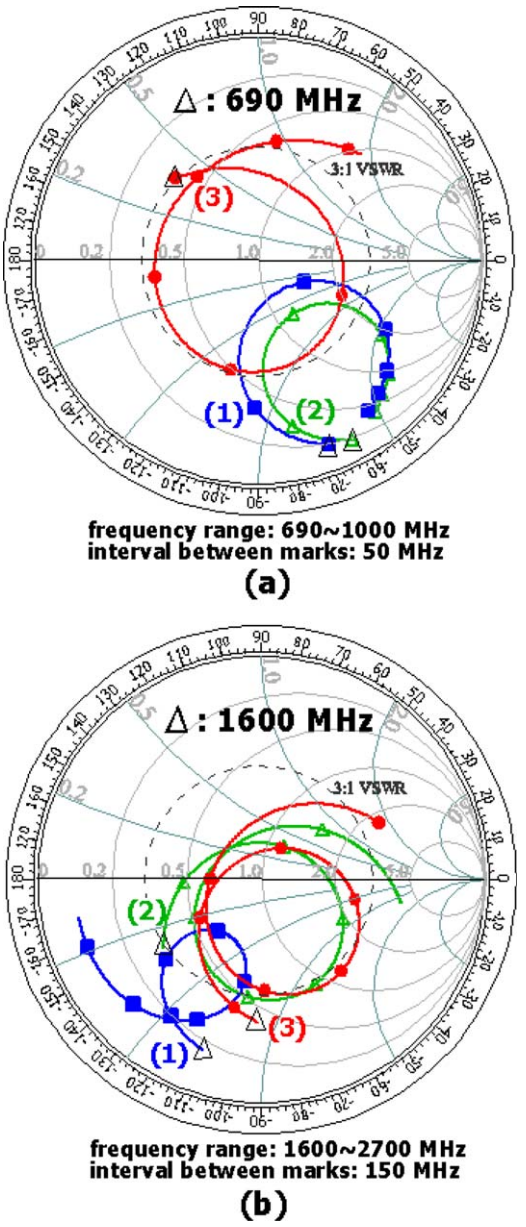

Figure 5 Simulated input impedance on the Smith chart for Ant1 (curve 1), Ant2 (curve 2), and the proposed antenna (curve 3). (a) Frequency range: 690–1000 MHz and (b) frequency range: 1600–2700 MHz. [Color figure can be viewed in the online issue, which is available at wileyonlinelibrary.com]

the higher band [see Fig. 5(b)], the tuning inductor leads to dual resonance for the input impedance in the desired higher band (curve 2 vs. curve 1), while the high-pass matching circuit shows small effects on the antenna's high-band performance (curve 3 vs. curve 2). The results conclude that the antenna's lower and higher bands can be controlled by the tuning inductor and the high-pass matching circuit, respectively.

4. PARAMETRIC STUDY

Effects of the major parameters of the coupling feed on the antenna performance are also studied. Figure 6 shows the simulated return loss for the proposed antenna as a function of the gap width g in the coupling feed. Results for the gap width varied from 0.3 to 0.5 mm are presented. When a larger gap width

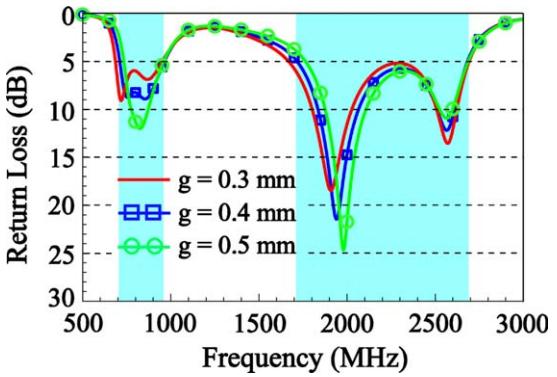

Figure 6 Simulated return loss for the proposed antenna as a function of the gap width g in the coupling feed. [Color figure can be viewed in the online issue, which is available at wileyonlinelibrary.com]

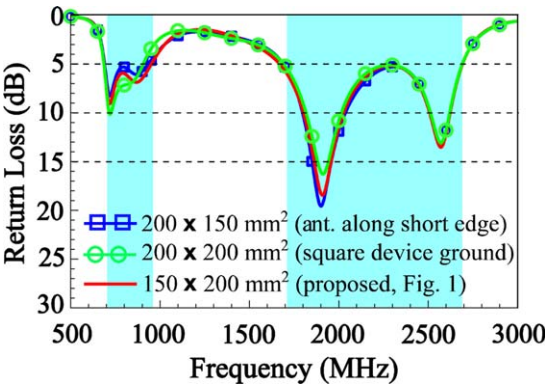

Figure 8 Simulated return loss for the proposed antenna with different device ground plane sizes. [Color figure can be viewed in the online issue, which is available at wileyonlinelibrary.com]

is used (e.g., $g = 0.5$ mm), the quarter-wavelength loop mode and the first higher-order loop mode will be slightly shifted to higher frequencies. In this case, the antenna cannot cover the desired LTE dual-wideband operation. A proper gap width (the selected gap width is 0.3 mm in the proposed design) is hence important in achieving the desired LTE dual-wideband operation.

Figure 7 shows the simulated return loss for the proposed antenna as a function of the length t of section BB′ in the coupling feed. Results for the length t varied from 9.5 to 11.5 mm are presented. When a shorter length t is used (for example, $t = 9.5$ mm), the three loop modes are all slightly shifted to higher frequencies. Effects on the quarter-wavelength loop mode and the first higher-order loop mode are similar to those observed for the gap width variations in Figure 6. For the effect on the second higher-order loop mode, it is very likely that the variations of the length t will also cause variations in the effective input inductance seen at the feeding port. This effect is similar to that of the tuning inductor L_1, thus causing some effects on the second higher-order loop mode. In the proposed design, the preferred length t is selected to be 11.5 mm.

Effects of the device ground plane sizes on the antenna performance are also studied. Figure 8 shows the simulated return loss for the proposed antenna with different device ground plane sizes of 200 × 150 mm^2 (the antenna mounted along the short edge), 200 × 200 mm^2 (a square device ground plane), and 150 × 200 mm^2 (the case in Fig. 1). Note that the proposed antenna is mounted along the long edge and flushed to one corner of device ground plane. When the antenna is mounted along the short edge and flushed to one corner of the device ground plane, the simulated return losses for the two cases are very similar.

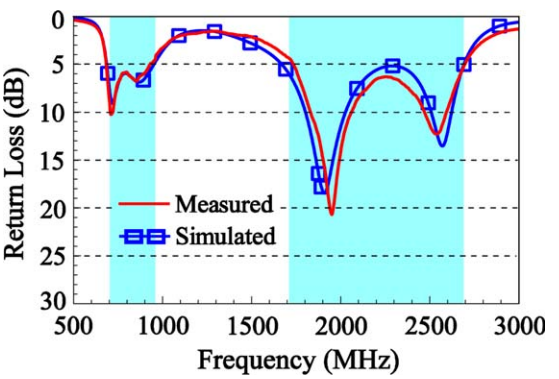

Figure 9 Measured and simulated return losses of the fabricated antenna. [Color figure can be viewed in the online issue, which is available at wileyonlinelibrary.com]

Conversely, when the antenna is mounted along one edge and flushed to one corner of a square device ground plane, relatively large effect on the impedance matching in the lower band

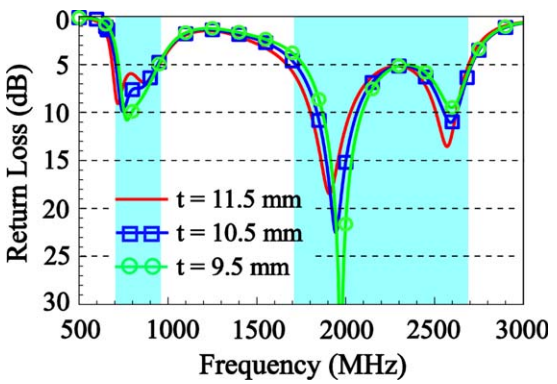

Figure 7 Simulated return loss for the proposed antenna as a function of the length t in the coupling feed. [Color figure can be viewed in the online issue, which is available at wileyonlinelibrary.com]

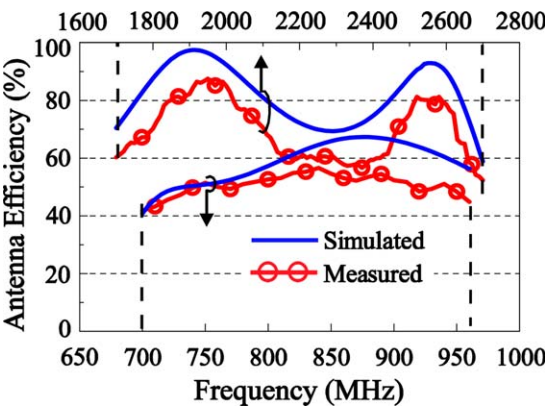

Figure 10 Measured and simulated antenna efficiencies of the fabricated antenna. [Color figure can be viewed in the online issue, which is available at wileyonlinelibrary.com]

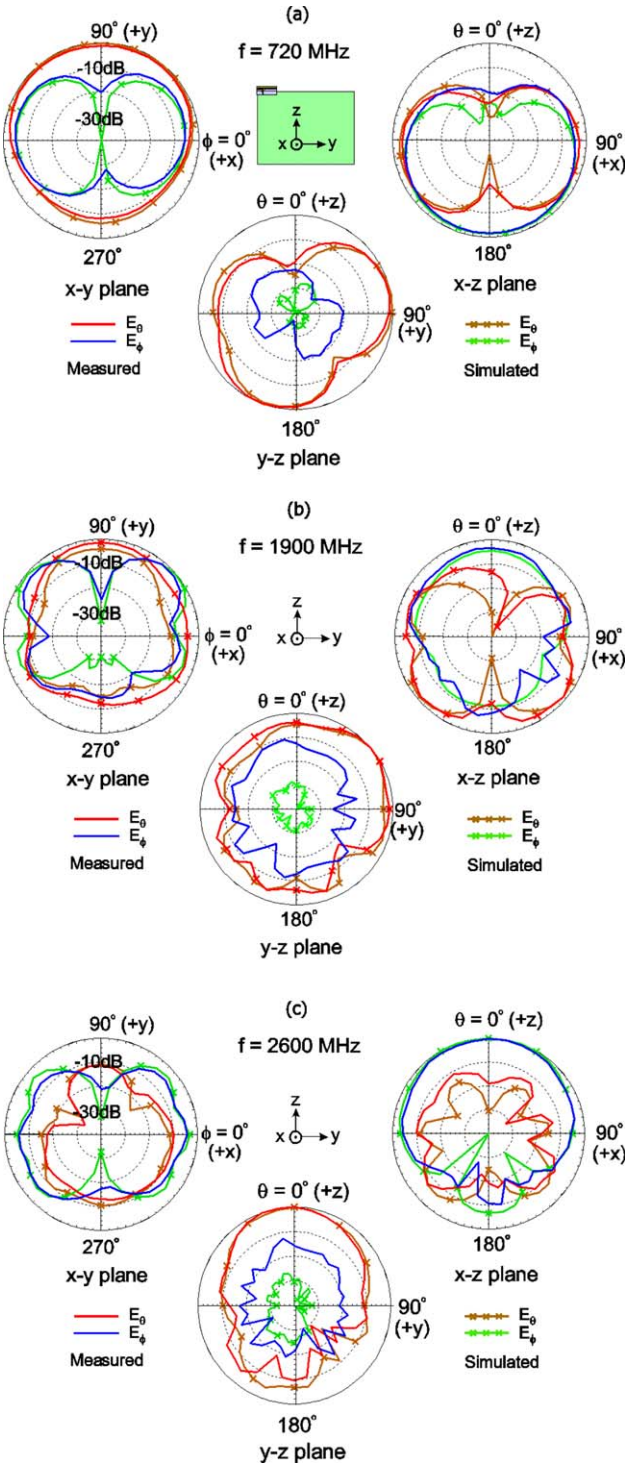

Figure 11 Measured and simulated radiation patterns of the fabricated antenna at 720, 1900, and 2600 MHz. [Color figure can be viewed in the online issue, which is available at wileyonlinelibrary.com]

is seen, with very small effects seen in the higher band. The results indicate that the variations in the device ground plane size of the tablet computer have small effects on the antenna's high-band performance. Conversely, effects of the device ground plane size on the antenna's low-band performance should be considered. In addition, as the results for the two cases of 200 × 150 mm^2 and 150 × 200 mm^2 are similar, it suggests that the antenna can be mounted along the short edge or long edge of a same device ground plane with small variations in the impedance matching.

5. EXPERIMENTAL RESULTS

The proposed antenna was fabricated and tested. Figure 9 shows the measured and simulated return losses of the fabricated antenna. Good agreement between the measurement and simulation is seen. The fabricated antenna can cover the LTE dual-wideband operation. The measured and simulated antenna efficiencies are shown in Figure 10. The antenna was measured in a far-field anechoic chamber. The measured efficiencies are, respectively about 40–56% and 56–88% in the lower and higher bands, which are acceptable for mobile communication applications [11]. Some discrepancies between the measured and simulated antenna efficiencies are also noted. The discrepancies may be owing to the ohmic losses associated with the three lumped circuit elements, which are not included in the simulation study.

Figure 11 shows the measured and simulated radiation patterns of the fabricated antenna at 720, 1900, and 2600 MHz. The radiation patterns at the horizontal plane (*x*-*y* plane) and two elevation planes (*x*-*z* and *y*-*z* planes) are shown, and the radiation intensities in the three principal planes are all normalized with respect to the same maximum intensity. Agreement between the measured data and simulated results is seen. At 720 MHz (a representative frequency in the lower band), the E_θ radiation is close to omnidirectional in the *x*-*y* plane. Stronger radiation in the lower-half planes of the elevation planes is also seen. The results indicate that the device ground plane also contributes to the radiation in the antenna's lower band. At 1900 and 2600 MHz (representative frequencies in the higher band), larger variations in the radiation patterns are seen. In addition, contrary to the observation at 720 MHz in the lower band, stronger radiation in the upper-half plane of the elevation plane at 2600 MHz is seen. The results indicate that the device ground plane acts like a reflector at higher frequencies. Also, in the higher band, comparable E_θ and E_ϕ radiation are seen in the *x*-*y* plane, which is good for mobile communications in complex propagation environments.

6. CONCLUSION

A very-low-profile loop antenna with a small size to provide dual-wideband operation for the LTE tablet computer has been proposed. The loop antenna occupies a volume of 8 × 3 × 40 mm^3 and uses a wideband feed structure consisting of a coupling feed, a high-pass matching circuit, and a tuning inductor to achieve the desired LTE dual-wideband operation in the 698–960 and 1710–2690 MHz bands. Detailed working principle of the wideband feed structure has been addressed. Good radiation characteristics in the two wide operating bands have also been obtained. The proposed antenna is promising for applications in modern slim tablet computers with a narrow spacing between the display panel and the device frame thereof.

REFERENCES

1. K.L. Wong and T.W. Weng, Very-low-profile dual-wideband tablet device antenna for LTE/WWAN operation, Microwave Opt Technol Lett 56 (2014), 1938–1942.
2. K.L. Wong and W.J. Lin, WWAN/LTE printed slot antenna for tablet computer application, Microwave Opt Technol Lett 54 (2012), 44–49.
3. Y.L. Ban, S.C. Sun, J.L.W. Li, and W. Hu, Compact coupled-fed wideband antenna for internal eight-band LTE/WWAN tablet computer applications, J Electromagn Waves Appl 26 (2012), 2222–2233.

4. S.H. Chang and W.J. Liao, A broadband LTE/WWAN antenna design for tablet PC, IEEE Trans Antennas Propag 60 (2012), 4354–4359.
5. W.S. Chen and W.C. Jhang, A planar WWAN/LTE antenna for portable devices, IEEE Antennas Wireless Propag 12 (2013), 19–22.
6. K.L. Wong and T.W. Weng, Small-size triple-wideband LTE/WWAN tablet device antenna, IEEE Antennas Wireless Propag Lett 12 (2013), 1516–1519.
7. K.L. Wong, H.J. Jiang, and T.W. Weng, Small-size planar LTE/WWAN antenna and antenna array formed by the same for tablet computer application, Microwave Opt Technol Lett 55 (2013), 1928–1934.
8. J.H. Lu and Y.S. Wang, Internal uniplanar antenna for LTE/GSM/UMTS operation in a tablet computer, IEEE Trans Antennas Propag 61 (2013), 2841–2846.
9. P.W. Lin and K.L. Wong, Dual-feed small-size LTE/WWAN strip monopole antenna for tablet computer applications, Microwave Opt Technol Lett 55 (2013), 2571–2576.
10. J.H. Lu and F.C. Tsai, Planar internal LTE/WWAN monopole antenna for tablet computer application, IEEE Trans Antennas Propag 61 (2013), 4358–4363.
11. K.L. Wong and M.T. Chen, Small-size LTE/WWAN printed loop antenna with an inductively coupled branch strip for bandwidth enhancement in the tablet computer, IEEE Trans Antennas Propag 61 (2013), 6144–6151.
12. K.L. Wong and T.W. Weng, Coupled-fed shorted strip antenna with an inductively coupled branch strip for low-profile, small-size LTE/WWAN tablet computer antenna, Microwave Opt Technol Lett 56 (2014), 1041–1046.
13. K.L. Wong and L.Y. Chen, Coupled-fed inverted-F antenna using an inverted-F coupling feed for small-size LTE/WWAN tablet computer antenna, Microwave Opt Technol Lett 56 (2014), 1296–1302.
14. K.L. Wong and P.W. Lin, Low-profile multi-branch monopole antenna with integrated matching circuit for LTE/WWAN/WLAN operation in the tablet computer, Microwave Opt Technol Lett 56 (2014), 1662–1666.
15. K.L. Wong and L.Y. Chen, Small-size LTE/WWAN tablet device antenna with two hybrid feeds, IEEE Trans Antennas Propag 62 (2014), 2926–2934.
16. Y.W. Chi and K.L. Wong, Quarter-wavelength printed loop antenna with an internal printed matching circuit for GSM/DCS/PCS/UMTS operation in the mobile phone, IEEE Trans Antennas Propag 57 (2009), 2541–2547.
17. Y.W. Chi and K.L. Wong, Very-small-size printed loop antenna for GSM/DCS/PCS/UMTS operation in the mobile phone, Microwave Opt Technol Lett 51 (2009), 184–192.
18. K.L. Wong, W.Y. Chen, and T.W. Kang, On-board printed coupled-fed loop antenna in close proximity to the surrounding ground plane for penta-band WWAN mobile phone, IEEE Trans Antennas Propag 59 (2011), 751–757.
19. Y.W. Chi and K.L. Wong, Compact multiband folded loop chip antenna for small-size mobile phone, IEEE Trans Antennas Propag 56 (2008), 3797–3803.
20. ANSYS HFSS, Ansoft Corp., Pittsburgh, PA, Available at: http://www.ansys.com/products/hf/hfss/.
21. S. Jeon, Y. Liu, S. Ju, and H. Kim, PIFA with parallel resonance feed structure for wideband operation, Electron Lett 47 (2011), 1263–1265.
22. S. Jeon and H. Kim, Mobile terminal antenna using a planar inverted-E feed structure for enhanced impedance bandwidth, Microwave Opt Technol Lett 54 (2012), 2133–2139.
23. K.L. Wong, Y.W. Chang, and S.C. Chen, Bandwidth enhancement of small-size WWAN tablet computer antenna using a parallel-resonant spiral slit, IEEE Trans Antennas Propag 60 (2012), 1705–1711.
24. K.L. Wong, T.J. Wu, and P.W. Lin, Small-size uniplanar WWAN tablet computer antenna using a parallel-resonant strip for bandwidth enhancement, IEEE Trans Antennas Propag 61 (2013), 492–496.

A HIGHLY TRANSPARENT BROADSIDE PATCH ANTENNA

Shaopeng Wan and Kama Huang
College of Electronics and Information Engineering, Sichuan University, Chengdu, Sichuan 610065, China; Corresponding author: kmhuang@scu.edu.cn

Received 5 June 2014

ABSTRACT: *The transparent antenna can potentially be combined with solar cells to create multifunctional compact systems. In this article, an optically transparent broadside antenna is presented. Based on a meshed patch antenna which has three horizontal lines and three vertical lines, the antenna has four more lines to increase the bandwidth. The antenna is fed by a top fed for simple structure, and the area of the feed line is much smaller than the one of a side fed. The transparency is much better because of the low ratio of metal area, which can be further reduced without destroying the performance of the antenna. The transparent broadside antenna is studied at 2.5 GHz. On the upper surface of the antenna, the ratio of metal area is 3.2%, and the measured −10 dB impedance bandwidth is close to 60 MHz.* © 2015 Wiley Periodicals, Inc. Microwave Opt Technol Lett 57:146–149, 2015; View this article online at wileyonlinelibrary.com. DOI 10.1002/mop.28801

Key words: *meshed patch antennas; transparency; broadside; radiation patterns*

1. INTRODUCTION

The advantages of optically transparent antennas make them can be integrated with clear substrates such as window glass for security and aesthetics [1], and there will be more applications if they are integrated with solar cell. Combining a GPS patch antenna with silicon solar cells for vehicular systems have already been studied [2]. A solar monopole antenna for low-power UMB transceivers and a microstrip patch antenna integrated with polycrystalline silicon solar cell have also been put into practice [3,4]. Combining transparent patch antennas with solar cells can also save the surface real estate of small satellites and be potentially used as embedded elements within WLAN/WiMAX communication systems [5,6].

In general, there are two ways to make the antennas achieve optical transparency: use of meshed conductor, such as meshed antennas; use of transparent conductor, such as indium tin oxide (ITO) and AgHT. For an S-band transparent antenna, meshed antennas can provide 90% transparency and more than 50% efficiency. However, for transparency higher than 70%, ITO or AgHT can only provide an antenna efficiency of less than 40%. With the increment of frequency, the efficiency of ITO films antennas may improve. On the contrary, the efficiency may reduce for meshed antennas due to the increased leaking of high frequency microwave signals through the mesh [7].

The antenna described in this article belongs to the first class, the only difference is that four lines are added on the basis of a meshed patch antenna, which has three horizontal lines and three vertical lines to increase the bandwidth of the antenna. Although the antenna was studied and fabricated on nontransparent substrate, the design method is the same for transparent and nontransparent substrates. The antenna has a simpler structure and better transparency than most transparent antennas, meanwhile, the performance of the antenna is good.

2. ANTENNA DESIGN

In the simulation, the initial antenna was a meshed patch antenna, which has three horizontal lines and three vertical lines,